Langmuir

Article

pubs.acs.org/Langmuir

Initial Step of pH-Jump-Induced Lamellar to Bicontinuous Cubic Phase Transition in Dioleoylphosphatidylserine/Monoolein

Toshihiko Oka,[†,‡] Taka-aki Tsuboi,[‡] Takahiro Saiki,[‡] Tomoki Takahashi,[‡] Jahangir Md. Alam,[†] and Masahito Yamazaki*[,†,‡,§]

[†]Nanomaterials Research Division, Research Institute of Electronics, [‡]Department of Physics, Graduate School of Science, and [§]Integrated Bioscience Section, Graduate School of Science and Technology, Shizuoka University, Shizuoka 422-8529, Japan

ABSTRACT: Electrostatic interactions (EI) are an important factor for phase transitions between lamellar liquid-crystalline (L_α) and inverse bicontinuous cubic (Q_{II}) phases. We investigated the low pH-induced L_α to double-diamond cubic (Q_{II}^D) phase transition in dioleoylphosphatidylserine (DOPS)/monoolein (MO) using time-resolved small-angle X-ray scattering. Using a stopped-flow apparatus, a suspension of liposomes (multilamellar vesicles (MLVs) or large unilamellar vesicles (LUVs)) of 20%-DOPS/80%-MO membrane at neutral pH was rapidly mixed with a low pH buffer, and then the structural change of the membranes in the resultant suspension was observed as a function of time (i.e., pH-jump experiment). At the initial step, the L_α phase was directly transformed into the hexagonal II (H_{II}) phase, and subsequently, the H_{II} phase slowly converted into the Q_{II}^D phase. We obtained the rate constants of the initial step (i.e., the L_α to H_{II} phase transition) and of the second step (i.e., the H_{II} to Q_{II}^D phase transition) using the non-negative matrix factorization method. The rate constant of the initial step was independent of the MLV concentration, indicating that single MLVs can convert into the H_{II} phase without any interaction with other MLVs. On the other hand, the rate constant of the initial step increased with a decrease in pH, 0.041 s^{-1} at pH 2.6 and 0.013 s^{-1} at pH 2.8, and also exhibited a size dependence; for smaller vesicles such as LUVs and smaller MLVs with diameters of ~1 μm, the rate constant was smaller. They were reasonably explained by the classical nucleation theory. These results provide the first experimental evidence of the total kinetics of EI-induced L_α/Q_{II} phase transitions.

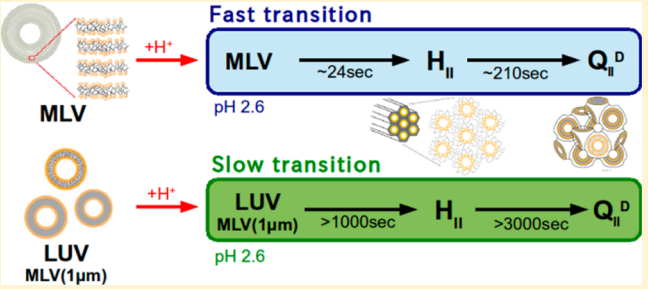

1. INTRODUCTION

Biomembranes and lipid membranes are usually in the lamellar liquid-crystalline (L_α) phase. In particular, multilamellar vesicles (MLVs) of these membranes have onionlike structures in which many bilayers are arranged regularly with the same aqueous intermembrane space. However, under certain conditions, lipids form cubic (Q) phases, where the membranes are connected in three-dimensional space with a cubic symmetry.[1−4] The inverse bicontinuous cubic (Q_{II}) phases (e.g., the double-diamond Q_{II}^D (or Q^{224}), the Q_{II}^P (or Q^{229}), and the gyroid Q_{II}^G (or Q^{230}) phase) have an infinite periodic minimal surface consisting of bicontinuous regions of water and hydrocarbon.[1] To date, the effects of temperature, water content, and pressure on the phase transitions between the L_α and the Q_{II} phases and on the intercubic phase transitions have been investigated, but these severe physical conditions are generally lethal to cells. We found a mild factor to induce these phase transitions, that is, the electrostatic interactions due to the surface charges of biological lipid membranes.[5,6] Subsequently, other examples of the modulation of electrostatic interaction (EI)-induced L_α/Q_{II} phase transitions, and transitions between different Q_{II} phases in various lipids, were reported.[7−20] Recently using small-angle X-ray scattering (SAXS), we found that low pH-induced transitions from the L_α to Q_{II}^D phase occur in dioleoylphosphatidylserine (DOPS)/monoolein (MO) membranes in the presence of poly(ethylene glycol)-6000 (PEG-6K).[13] This is an EI-induced phase transition, since the low pH decreases the surface charge density of these membranes, which induces the phase transition. DOPS and MO are essential biological lipids. pH is known to control the function and structure of membranes and proteins, thus playing an indispensable role in cells. This phase transition has therefore attracted much attention from both the physical and biological points of view.

To reveal the mechanism behind the L_α/Q_{II} phase transitions, it is important to elucidate the kinetic pathway. The kinetics of the temperature (T)-jump or pressure (P)-jump-induced L_α to Q_{II} phase transitions or intercubic phase transitions and also the T-scan- (i.e., the continuous T change-) induced phase transitions in various lipids has been investigated using time-resolved SAXS (TR-SAXS).[21−28] For example, Conn et al. investigated the T- (or P-) jump-induced L_α to Q_{II}^D phase transition in monoelaidin using TR-SAXS, and found several intermediates during the transition.[26] For the EI-induced L_α/Q_{II} phase transitions, we investigated the kinetics of the low pH-induced L_α to Q_{II}^D phase transition in DOPS/MO in the

Received: February 14, 2014
Published: June 20, 2014

   dx.doi.org/10.1021/la5021719 | *Langmuir* 2014, 30, 8131−8140

presence of PEG-6K using TR-SAXS. We found that the H_{II} phase appeared as an intermediate structure within 2 s after mixing a low pH buffer; subsequently the H_{II} phase slowly converted into the Q_{II}^{D} phase.[21] However, since the time resolution of this method is 2 s, we could not reveal in detail the initial step of this phase transition, nor its kinetics.

In this study, we investigated the initial step of the low pH-induced L_α to Q_{II}^{D} phase transition in 20%-DOPS/80%-MO in the absence of PEG-6K. In particular, we wanted to determine whether the L_α phase converts directly to the H_{II} phase or via another intermediate, and also to obtain detailed information on the kinetics of this conversion. To increase the time resolution of the TR-SAXS measurement, we used a stopped flow apparatus for rapid mixing, which has only 10 ms of the dead time. PEG-6K could not be used with this apparatus, because it induces rapid association of the MLVs which could block the narrow tubes in the apparatus. Using the stopped-flow apparatus, a suspension of liposomes (multilamellar vesicles (MLVs) or large unilamellar vesicles (LUVs)) of 20%-DOPS/80%-MO membrane at neutral pH was rapidly mixed with a low pH buffer, and then the structural change of the membranes in the resultant suspension was observed as a function of time using TR-SAXS (i.e., pH-jump experiment). Based on these results, we herein report the structural changes occurring in DOPS/MO membranes 10 ms after pH-jump with a time resolution of 200 ms.

2. MATERIALS AND METHODS

MO was purchased from Sigma Chemical Co. (St. Louis, MO). DOPS and 1,2-dioleoyl-*sn*-glycero-3-phosphethanolamine-*N*-(7-nitro-2-1,3-benzoxadiazole-4yl) (NBD-DOPE) were purchased from Avanti Polar Lipids (Alabaster, AL). To prepare DOPS/MO-MLVs, 500 μL of 10 mM ammonium acetate buffer (pH 6.7) containing 100 mM NaCl (buffer A) was added to the dry MO/DOPS lipid film (50 μmol),[21] and then the suspension was mixed several times using a vortex mixer for about 20 s at room temperature (~25 °C). To purify MLVs, the MLV suspension was centrifuged at 13 000*g* for 20 min at 25 °C, then the pellet was resuspended gently in new buffer A without using the vortex mixer. We used this suspension as the purified MLV suspension. To prepare DOPS/MO-LUVs, the MLV suspension was extruded through a 100 nm pore size nuclepore membrane using the extrusion method.[13] The purified MLVs and LUVs were used within 12 h of preparation. The lipid concentrations of the suspensions were determined by the Bartlett method.

TR-SAXS data were obtained at the BL40B2 or BL45XU beamlines at SPring-8 (Sayo, Japan). The X-ray wavelength used was 0.1000 nm, and the camera length was 1150 mm. Data were collected using a two-dimensional pixel array detector (PILATUS 100 K, DECTRIS, Baden, Switzerland). A stopped flow apparatus (SFM-CD10, UNISOKU, Osaka, Japan) was used to mix rapidly the purified DOPS/MO-MLV (or LUV) suspension in buffer A with 20 mM citrate buffer at various pH values containing 100 mM NaCl (buffer C) at a volume ratio of 1:9. We arranged the stopped flow apparatus transversely and thereby the capillary cell was positioned horizontally. The temperature of the apparatus was kept at 25 °C with a water bath circulator (RTE111, Thermo Neslab, Newington, NH). TR-SAXS measurements were started following the mixing time of the stopped flow apparatus. The SAXS patterns were recorded for the first 60 s with a resolution of 0.2 s, then for 9 s with a resolution of 0.2 s at various intervals for a total of 3629 s from the mixing time. The stopped flow apparatus was moved during the X-ray exposure to avoid damage of the sample caused by the X-ray irradiation. A series of sequential two-dimensional ring diffraction patterns were averaged circularly to reduce them into a set of sequential one-dimensional patterns. These patterns were corrected by subtracting the background scatter caused by the capillary and the buffer.

The sequential one-dimensional diffraction patterns are equivalent to the matrix $X(S, t)$, in which the matrix element X_{ij} corresponds to the intensity at the ith scattering vector S_i and jth delay-time t_j. The $m \times n$ matrix X is the product of the $m \times k$ matrix of the pure component diffraction profiles A, and $n \times k$ matrix of the concentration time courses B, where k is the number of components,

$$X = AB^T + E$$

where the superscript T denotes the transpose of the matrix. E is the residual matrix containing the data variance or statistical noise which is not explained by AB^T. To analyze matrix X, we applied a non-negative matrix factorization (NMF) method based on a modified alternating least-squares (MALS) algorithm.[29,30] In a typical MALS algorithm, optimized values of A and B are calculated from a random matrix alternatingly with the constraint that the values in A and B are non-negative. Given fluctuations in the data, we adopted two constraints as follows: (1) the mean values of the adjacent points are non-negative for matrix A or larger than -1σ for matrix B; (2) the mean value of the first points in matrix B without a first component is within $\pm 1\sigma$. The parameter σ is the standard deviation of data in corresponding region. The program is coded on GNU Octave. We used a k value of 3, which is the number of components we could distinguish from the contour maps. Data up to 330 s were used in the calculations. We repeated independent MALS calculations more than 10 times. Converged matrices A from the independent calculations were almost identical; this was also true for the B matrices.

The MLVs of 20%-DOPS/79%-MO/1%-NBD-DOPE in buffer A were observed using a confocal laser scanning microscope (CLSM; FV-1000, Olympus, Tokyo, Japan) or an inverted differential interference contrast microscope (DIC; IX-71, Olympus) at 25 ± 1 °C using a stage thermocontrol system (Thermoplate, Tokai Hit, Shizuoka, Japan). Giant unilamellar vesicles (GUVs) of 40% dioleoylphosphatidylglycerol (DOPG), 59% dioleoylphosphatidylcholine (DOPC), and 1% NBD-DOPE mixture were prepared in PIPES buffer (10 mM PIPES, pH 7.0, 150 mM NaCl, 1 mM EGTA) using the standard method,[31] and were observed using the CLSM. The size of the LUVs was measured at 25 °C using a dynamic light scattering (DLS) apparatus (Zetasizer Nano ZS, Malvern Instrument Ltd., Worcester, U.K.). The average particle diameter (*Z*-average) of the LUVs was obtained by the cumulant method.

3. RESULTS

3.1. The Kinetics of the Low pH-Induced L_α to Q_{II}^{D} Phase Transition in MLVs. First, the kinetics of the low pH-induced L_α to Q_{II}^{D} phase transition in MLVs of 20%-DOPS/80%-MO (molar ratio) at a final pH of 2.6 was investigated at 25 °C. The SAXS pattern of 6.3 mM purified MLVs of this membrane in buffer A (pH 6.7) indicated that the membrane was in the L_α phase with a spacing of 9.8 nm (Figure 1a). The SAXS peaks are very broad, indicating a short scattering correlation length. The 20%-DOPS/80%-MO-MLVs have the large spacing due to the electrostatic repulsion between charged neighboring membranes and also the membrane is in the L_α phase, and thereby a large thermal fluctuations of membrane (i.e., the undulation motion) exists. It is well-known that such undulation motion decreases the long-range positional correlation of the membranes inside a MLV to increase the width of the SAXS peak, and thus the broad SAXS peaks were observed in charged lipid membranes.[32,33] Since the lipid concentration is 0.5 wt %, and thus the swelling of the MLV is not limited by the amount of water. This indicates that the large spacing of 9.8 nm in the MLV is determined by a minimum of the interbilayer interaction potential. These results show that the bilayers in the MLV are weakly bound.[32,33] To confirm the structure of the L_α phase, we observed the MLVs using microscopy. Figure 2a shows a DIC image of the MLVs whose diameters are 5−10 μm. A CLSM image of the MLVs containing a fluorescent lipid, NBD-DOPE, shows that the interior of the vesicle has homogeneously strong fluorescence intensity (Figure 2b), indicating that in the inside of

dx.doi.org/10.1021/la5021719 | *Langmuir* 2014, 30, 8131−8140

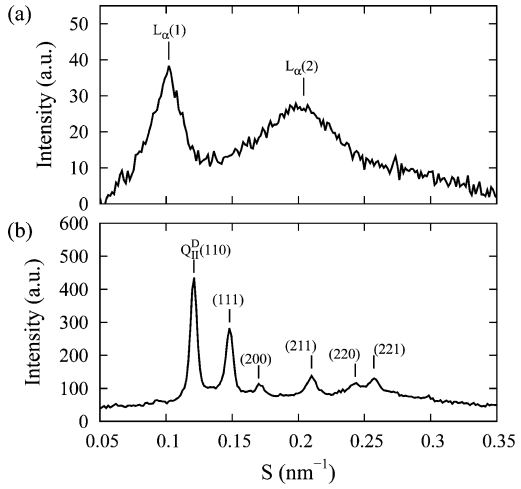

Figure 1. SAXS patterns of a 6.3 mM 20%-DOPS/80%-MO-MLV suspension (a) in buffer A (pH 6.7) and (b) in mixed buffer at pH 2.6 after a long incubation time of 10 h.

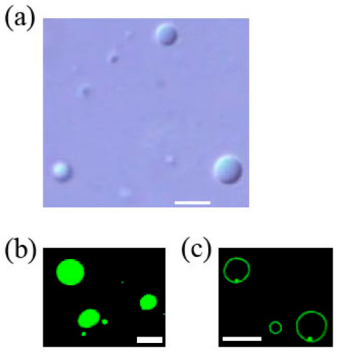

Figure 2. (a) DIC images of 20%-DOPS/80%-MO-MLVs. Scale bar is 10 μm. (b) CLSM image of 20%-DOPS/79%-MO/1%-NBD-DOPE-MLVs. Scale bar is 10 μm. (c) CLSM image of 40%-DOPG/59%-DOPC/1%-NBD-DOPE-GUVs. Scale bar is 10 μm.

the vesicle there are many bilayers because we can observe only the cross section of the vesicle using CLSM. In comparison to this, a CLSM image of 40%-DOPG/60%-DOPC-GUVs shows that only the rim of the vesicles has fluorescence intensity because the GUVs are unilamellar vesicles (Figure 2c). The results obtained using microscopy clearly indicate that the membranes form the MLV structure. Moreover, to prepare the purified MLVs, we centrifuged the suspension of membranes using weak centrifugal force (13 000*g* for 20 min) and obtained a pellet of membranes. Therefore, the above results indicate that 20%-DOPS/80%-MO membranes form the MLVs of the membrane in L_α phase. After the purified MLV suspension in buffer A was rapidly mixed with buffer C (pH 2.4), the structure of the MLVs in the resultant suspension (6.3 mM lipid, final pH 2.6) changed with time. The contour plot shows the time course of the SAXS patterns of this sample (Figure 3a). From 0.2 to 10 s, only SAXS peaks corresponding to the MLVs (L_α phase) were observed (Figure 3a, b). At 10 s after mixing, a new weak peak appeared around $S = 0.165$ nm^{-1}, and its intensity increased with time. The SAXS pattern at 60 s (Figure 3a, b) had a spacing with a ratio $1:\sqrt{3}:2$, corresponding to the H_{II} phase, indicating that the peak at $S = 0.165$ nm^{-1} was due to (10) of the H_{II} phase. The intensities of the peaks of the H_{II} phase increased with time up to 60s and then decreased (Figure 3c), whereas those of the L_α

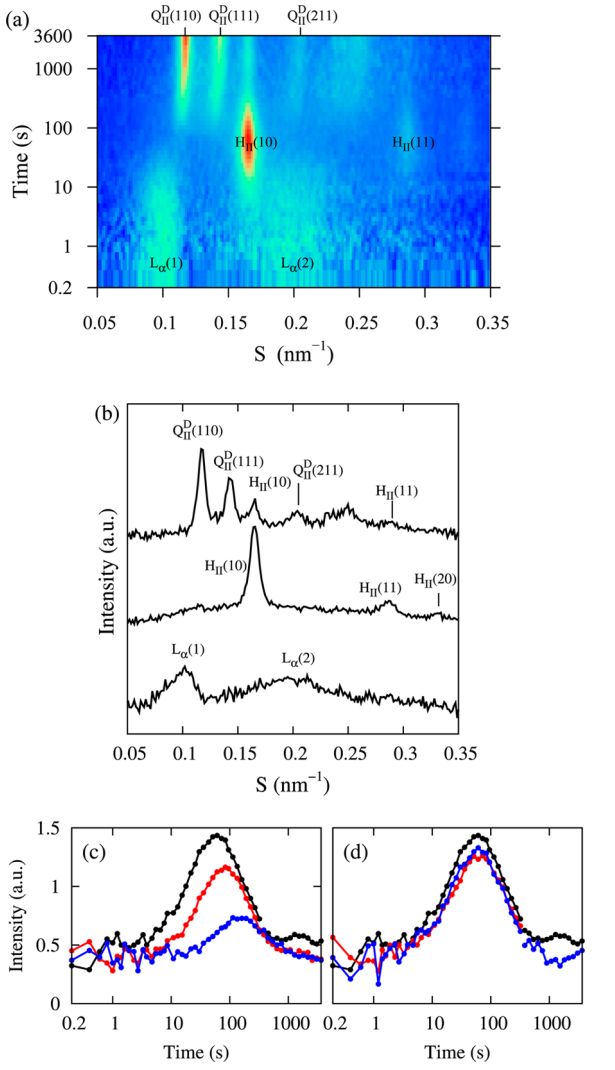

Figure 3. Changes in structure and phase of 20%-DOPS/80%-MO-MLVs after the pH-jump from pH 6.7 to low pH (6.3 mM lipid concentration). (a) A SAXS contour plot of the time course at pH 2.6. (b) Averaged SAXS patterns of the data shown in (a) from 0.2 to 2 s (bottom), from 1076 to 1085 s (middle), from 3620 to 3629 s (top). (c) Integrated intensity of the (10) peak of the H_{II} phase at pH 2.6 (black), 2.7 (red), and 2.8 (blue). The integrated region was from $S = 0.156$ to 0.170 nm^{-1}. The data up to 330 s are averaged values from several experiments. (d) Integrated intensity of the (10) peak of the H_{II} phase; at a lipid concentration of 6.3 mM (black), at 4.4 mM (red) and 3.2 mM (blue). Final pH values were 2.6. The integrated intensity was normalized to the sample concentration.

phase became low at 60 s. The SAXS patterns of the L_α phase don't have good S/N values and also its SAXS peaks are very broad, and thereby it is difficult to obtain information on the structural changes over time such as the spacing change before the transition. At 120 s, two weak peaks at $S = 0.113$ and 0.138 nm^{-1} appeared, then their intensities increased with time (Figure 3a, b). We also measured the SAXS pattern of the same sample following a long incubation (10 h) (Figure 1b); this pattern should correspond to the equilibrium structure. Indexing of the SAXS peaks indicated the existence of the Q_{II}^D phase. Peaks had spacings in the ratio $\sqrt{2}:\sqrt{3}:\sqrt{4}:\sqrt{6}:\sqrt{8}:\sqrt{9}:\sqrt{10}$, indexed as (110), (111), (200), (211), (220), (221), and (310) reflections of the Q_{II}^D phase; its lattice constant was 11.7 nm. Based on the equilibrium structure, the peaks at $S = 0.113$ and 0.138 nm^{-1} in

dx.doi.org/10.1021/la5021719 | *Langmuir* 2014, 30, 8131−8140

Figure 3a and b were assigned as the (110) and (111) peak of the Q_{II}^{D} phase.

The pH dependence of the kinetics of this phase transition was investigated. The qualitative characteristic of the transition at all pH values was the same as that shown in Figure 3a. Figure 3c shows the time course of the intensity of the (10) peak of the H_{II} phase, indicating that the rate constant of the conversion from the L_α to the H_{II} phase decreased with an increase in pH. The lattice parameters of the H_{II} and the Q_{II}^{D} phases increased as the pH increased (Table 1). We also investigated the effect of lipid concentration on the kinetics of this phase transition. The qualitative characteristic of the transition at all lipid concentrations was the same as that shown in Figure 3a. Figure 3d shows the time course of the intensity of the (10) peak of the H_{II} phase; the rate constant was almost the same, irrespective of the lipid concentration.

Table 1. pH Dependence of the Lattice Parameters

final pH	L_α (initial) [nm]	H_{II} (intermediate) [nm]	Q_{II}^{D} (final) [nm]
2.6	10.0	6.98	11.7
2.7	10.0	7.02	12.3
2.8	10.0	7.09	13.4

3.2. The Kinetics of the Low pH-Induced L_α to Q_{II}^{D} Phase Transition in LUVs and Smaller-Sized MLVs. Next we investigated the effects of the size of the vesicles on this phase transition. We used LUVs with diameters of 136 nm (*Z*-average) in buffer A. After the LUV suspension was rapidly mixed with buffer C (pH 2.4), the structure of the LUVs in the resultant suspension (8.5 mM lipid, final pH 2.6) changed with time (Figure 4a, b). At the beginning and up to 300 s, no SAXS peaks were observed. At 300 s after mixing, a new weak peak due to the H_{II} phase appeared at $S = 0.165$ nm^{-1}, and its intensity increased with time. In contrast with the results obtained with MLVs (Figure 3a), the rapid increase in SAXS peaks due to the H_{II} phase (10−100 s) was not observed. SAXS peaks due to MLVs were not observed before the appearance of the H_{II} phase, indicating that MLVs with many bilayers were not formed as an intermediate. The pH dependence of the kinetics of this structural transition was also investigated. The qualitative characteristic of the transition at all pH values was the same as that shown in Figure 4a. Figure 4c shows the time course of the intensity of the (10) peak of the H_{II} phase, and indicates that the rate constant of the formation of the H_{II} phase decreased with increasing pH. The DLS data indicate that the LUVs associated and thus increased in size with time under the same conditions as that of the TR-SAXS experiment (Figure 4d, e). The rate of the association decreased with increasing pH.

We obtained similar results for the low pH-induced transformation of smaller MLVs with diameters of ∼1 μm into the Q_{II}^{D} phase (Figure 5). The time course of the structural change shown in Figure 5a was almost the same as that shown in Figure 4a. Figure 5c shows the time course of the intensity of the (10) peak of the H_{II} phase, and indicates that the rate constant of the formation of the H_{II} phase decreased with increasing pH.

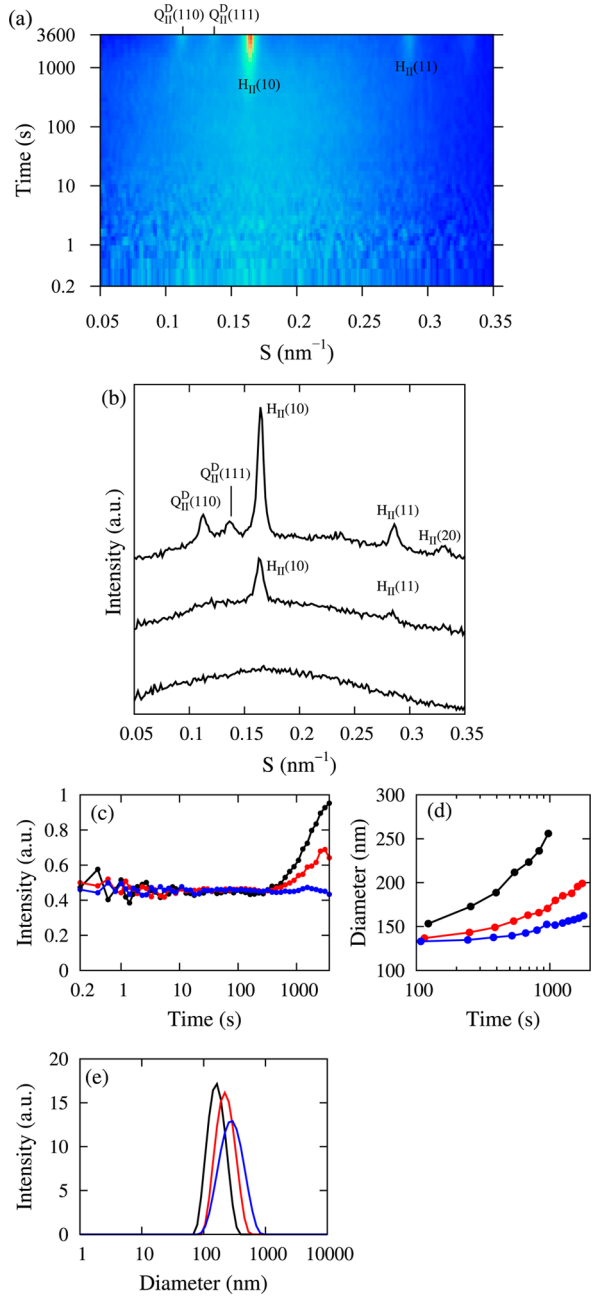

Figure 4. Changes in structure, phase, and size of 20%-DOPS/80%-MO-LUVs after the pH-jump from pH 6.7 to low pH (8.5 mM lipid concentration). (a) SAXS contour plot of the time course at pH 2.6. (b) Averaged SAXS patterns of the data shown in (a) from 0.2 to 2 s (bottom), from 1076 to 1085 s (middle), and from 3620 to 3629 s (top). (c) Integrated intensity of the (10) peak of the H_{II} phase. The integrated region was from $S = 0.156$ to 0.170 nm^{-1}. (d) Time course of the average particle diameter (*Z*-average) in the LUV suspension. The values of time represent medians of each measurement time. Final pH of 2.6 (black), 2.7 (red), and 2.8 (blue). (e) Size (diameter) distribution (by intensity) of 20%-DOPS/80%-MO-LUVs after the pH-jump from pH 6.7 to 2.6. The time after the pH-jump was 123 s (black), 543 s (red), and 973 s (blue), where these times represent medians of each measurement time. These distributions are averaged ones from 60 to 185 s (black), from 470 to 615 s (red), from 900 to 1045 s (blue). The size distributions were obtained using the non-negative least-squares method.

4. DISCUSSION

The above results clearly show the kinetic pathway of the low pH-induced L_α to Q_{II}^{D} phase transition. First, the L_α phase directly converts into the H_{II} phase in immediate response to the pH-jump (the initial step), then the H_{II} phase gradually converts into the Q_{II}^{D} phase. For the initial step, there are two patterns; one is the rapid appearance of the H_{II} phase which started around 10 s at pH 2.6 (Figure 3a), and the other is the slow appearance of

dx.doi.org/10.1021/la5021719 | *Langmuir* 2014, 30, 8131−8140

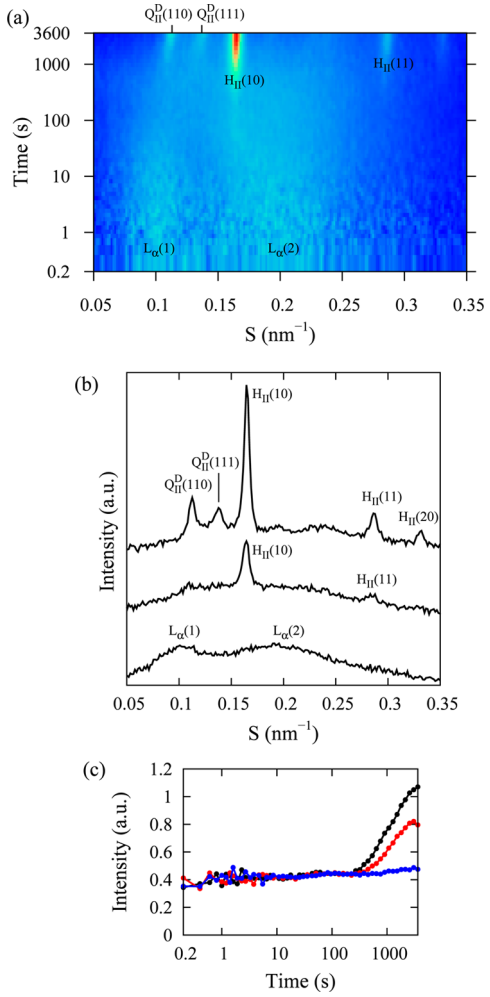

Figure 5. Changes in structure and phase of 20%-DOPS/80%-MO-MLVs with diameters of ~1 μm after the pH-jump from pH 6.7 to low pH (7.4 mM lipid concentration). (a) SAXS contour plot of the time course at a final pH of 2.6. (b) Averaged SAXS patterns of the data shown in (a) from 0.2 to 2 s (bottom), from 761 to 770 s (middle), from 3620 to 3629 s (top). (c) Integrated intensity of the (10) peak of the H_{II} phase; at pH 2.6 (black), 2.7 (red), and 2.8 (blue). The integrated region was from S = 0.156 to 0.170 nm^{-1}. To prepare DOPS/MO-MLVs with diameters of ~1 μm, the MLV suspension was extruded through a 1 μm pore size nuclepore membrane using a standard extrusion method.

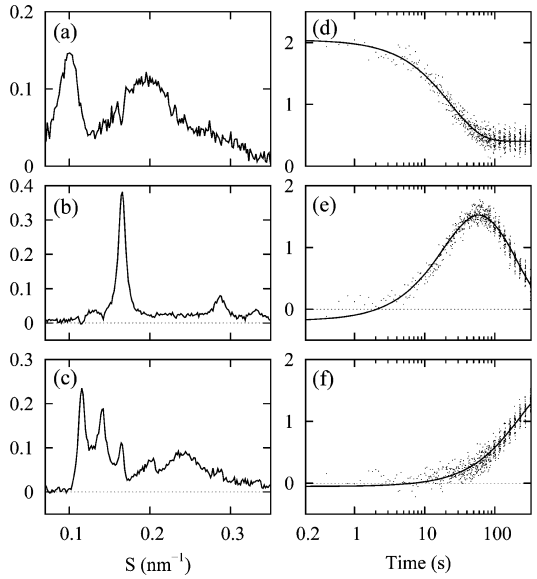

Figure 6. Results from the MALS calculations of the SAXS pattern of a 6.3 mM 20%-DOPS/80%-MO-MLV suspension after the pH-jump from pH 6.7 to 2.6 (Figure 3a). Restored SAXS profiles of matrix *A* corresponding to the L_α, the H_{II}, and the Q_{II}^{D} phases are shown in (a), (b), and (c), respectively. The time courses of the SAXS intensities of matrix *B* corresponding to the L_α, the H_{II}, and the Q_{II}^{D} phases are shown in (d), (e), and (f), respectively.

the H_{II} phase which started around 300 s (Figure 4a and 5a). For the MLVs, the rapid appearance was dominant, but for the LUVs only the slow appearance was observed. Using our TR-SAXS system, we can clearly detect the H_{II} phase peaks due to hexasomes with diameters of 100−200 nm at similar lipid concentrations. We can therefore reasonably conclude that the slow appearance of the H_{II} phase indicates the slow conversion to the H_{II} phase.

Next we analyzed the kinetics of this phase transition quantitatively. In the low pH-induced L_α to Q_{II}^{D} phase transition of the purified MLVs (e.g., Figure 3a), SAXS peaks due to each phase were well separated. We therefore applied the non-negative matrix factorization (NMF) method[29,30] to obtain the time course of each phase. The results of the NMF method are shown in Figure 6. Figure 6a−c indicates three components in the data, that is, the L_α (a), the H_{II} (b), and the Q_{II}^{D} phase (c). Figure 6d−e indicates the time course of each component. We can divide the time course into two stages. At the first stage up to around 50 s, the amount of the L_α phase decreased, the H_{II} phases increased, and the Q_{II}^{D} phase remained almost 0. Most of the membranes in the L_α phase, therefore, converted into the H_{II} phase. At the second stage from 50 to 300 s, the amount of the H_{II} phase decreased, the Q_{II}^{D} phase increased, and the L_α phase remained constant. Therefore, at the second stage, the phase transition occurred from the H_{II} to the Q_{II}^{D} phase. The basic scheme of the phase transitions is as follows:

$$L_\alpha \xrightarrow{k_1} H_{II} \xrightarrow{k_2} Q_{II}^{D} \quad (1)$$

where k_1 and k_2 are the rate constant of the transition from the L_α to the H_{II} phase and of the transition from the H_{II} to the Q_{II}^{D} phase, respectively. The time courses of the concentration of each phase are described using following differential equations.

$$\frac{d[L_\alpha]}{dt} = -k_1[L_\alpha]$$

$$\frac{d[H_{II}]}{dt} = k_1[L_\alpha] - k_2[H_{II}]$$

$$\frac{d[Q_{II}^{D}]}{dt} = k_2[H_{II}] \quad (2)$$

The solutions for these differential equations at the initial condition ($[L_\alpha] = C_0$ at $t = 0$) are as follows.

$$[L_\alpha] = C_0 \exp(-k_1 t)$$

$$[H_{II}] = \frac{k_1 C_0}{k_2 - k_1}\{\exp(-k_1 t) - \exp(-k_2 t)\}$$

$$[Q_{II}^{D}] = \frac{C_0}{k_2 - k_1}\{k_1 \exp(-k_2 t) - k_2 \exp(-k_1 t)\} + C_0 \quad (3)$$

dx.doi.org/10.1021/la5021719 | *Langmuir* 2014, 30, 8131−8140

The time courses in Figure 6 are not the fraction of components, and the values might not start from or end at 0. We modified the equations as follows:

$$[L_\alpha] = A_0 \exp(-k_1 t) + B_0$$
$$[H_{II}] = A_1\{\exp(-k_1 t) - \exp(-k_2 t)\} + B_1$$
$$[Q_{II}{}^{D}] = A_2\{k_1 \exp(-k_2 t) - k_2 \exp(-k_1 t)\} + B_2 \quad (4)$$

The time course of the SAXS intensities of the three phases (Figure 6d–f) was fit well by eq 4, providing $k_1 = 0.041\ s^{-1}$ and $k_2 = 0.0048\ s^{-1}$. These results indicate that the kinetic pathway of the low pH-induced L_α to $Q_{II}{}^{D}$ phase transition in 20%-DOPS/80%-MO membranes is $L_\alpha \rightarrow H_{II} \rightarrow Q_{II}{}^{D}$. The rate constant increased with a decrease in pH (Table 2). This result suggests that the activation energy for the L_α to the H_{II} phase decreases with decreasing pH. Table 3 shows that the rate constant of the initial step was independent of the MLV concentration (i.e., the lipid concentration), suggesting that the rate-determining step is not a diffusion-limited reaction, and thus is independent of collisions between MLVs. These results suggest that each MLV can convert into the H_{II} phase without any interaction with other MLVs. In contrast, for the low pH-induced conversion of the LUVs to the $Q_{II}{}^{D}$ phase, association of the LUVs is a necessary step for the formation of the H_{II} and the $Q_{II}{}^{D}$ phases.

Table 2. pH Dependence of the Rate Constants

final pH	k_1 [s^{-1}]	k_2 [s^{-1}]
2.6	0.041 ± 0.001	0.0048 ± 0.0001
2.7	0.021 ± 0.001	0.0048 ± 0.0002
2.8	0.013 ± 0.001	0.0032 ± 0.0002

Table 3. Lipid Concentration Dependence of the Rate Constants

final lipid concn [mM]	k_1 [s^{-1}]	k_2 [s^{-1}]
6.3	0.041 ± 0.001	0.0048 ± 0.0001
4.4	0.042 ± 0.001	0.0043 ± 0.0001
3.2	0.037 ± 0.001	0.0042 ± 0.0001

Comparing the current data with the findings described in our previous paper,[21] the rate of conversion of the L_α to the H_{II} phase in 20%-DOPS/80%-MO membrane in the presence of PEG-6K is much larger than in the absence of PEG-6K; in the presence of PEG-6K the conversion is complete less than 2 s. It is well established that PEG-6K induces the association of lipid vesicles.[21] Moreover, in the results described in the previous paper, the rapid formation of large aggregates of MLVs was observed by eye. These results suggest that the rate of conversion of the L_α to the H_{II} phase increases with an increase in the size of the membranes.

It is instructive to compare the intermediates and the rate constants (or the rate) of the low pH-induced phase transition of 20%-DOPS/80%-MO (i.e., the results in this report) with those of phase transitions of lipid membranes involved in nonlamellar phases such as the Q_{II} and the H_{II} phases. The first examples are the L_α to H_{II} phase transitions. Tate et al. found that in the T-jump-induced L_α to H_{II} phase transition of dioleoylphosphatidylethanolamine (DOPE) the lifetime τ of the L_α phase is 3 s (corresponding to the rate constant k of 0.3 s^{-1}) for a large temperature jump (from 3 °C to 24–37 °C), but with a decrease in magnitude of temperature jump the rate constant greatly decreases (e.g., $\tau = 6 \times 10^2$ s ($k = 0.002\ s^{-1}$) for a final temperature of 6 °C).[34] These transitions occurred without formation of any intermediates; that is, they are two-state transitions. During the transition the spacing of the H_{II} phase gradually increased with time from that of the L_α phase to the equilibrium spacing of the H_{II} phase, although the spacing the L_α phase did not change over time. In other T-jump-induced L_α to H_{II} phase transitions, similar results were obtained; the transitions are rapid and the lifetime of the L_α phase are order of 1–10 s.[35] On the other hand, the kinetics of the L_α to H_{II} phase transitions induced by compounds such as ions have not been well investigated. The initial step of the low pH-induced phase transition of 20%-DOPS/80%-MO (i.e., the L_α to H_{II} phase transition), which is one of the compound-induced phase transition, are slower than the T-jump-induced L_α to H_{II} phase transitions. We can reasonably consider that the rate-determining step of the compound-induced phase transition is the diffusion of compounds into the inside of MLVs. Compounds can enter the MLVs through a local defect or by passing through a lipid membrane directly. These elementary steps are not involved in the T-jump-induced phase transitions and also the P-jump-induced phase transition, and thereby the compound-induced phase transitions require more time compared with the T-jump- (or P-jump-) induced phase transitions. H^+ has the minimum size among all the compounds and thereby it can easily pass through the local defect of the MLV membranes. Moreover, H^+ can directly pass through the lipid membranes rapidly.[36] Therefore, we can reasonably consider that the H^+-induced phase transition has the largest rate constant among the compound-induced phase transitions in MLVs. The second examples are the L_α to Q_{II} phase transitions. Conn et al. investigated the T- (or P-) jump-induced L_α to $Q_{II}{}^{D}$ phase transition in monoelaidin.[26] The kinetic pathway of the P-jump-induced L_α to $Q_{II}{}^{D}$ phase transition from 1100 to 260 bar is complex: first the spacing of the L_α phase gradually decreased with time by 0.5 nm, and after a period of a few seconds the L_α phase converted to an unidentified intermediate with a broad, featureless scatter, then resolved itself into the intermediate $Q_{II}{}^{D}$ and $Q_{II}{}^{P}$ phases with a larger lattice constant (i.e., containing much water), and finally converted to the equilibrium $Q_{II}{}^{D}$ phase (at 80 s it started to appear, but at 30 min it coexisted with the $Q_{II}{}^{P}$ phase). In contrast, the kinetic pathway of the T-jump-induced L_α to $Q_{II}{}^{D}$ phase transition from 30 to 60 °C is simpler: first the spacing of the L_α phase gradually decreased with time by 0.2 nm, then the transition from the L_α to the $Q_{II}{}^{P}$ phase occurred, and finally the transition from the $Q_{II}{}^{P}$ to the $Q_{II}{}^{D}$ phase occurred around 15 min after the T-jump. The rate constants of these transitions were not determined. It is note that the kinetic pathways of the T-jump transition and that of the P-jump transition are different irrespective of the same L_α to $Q_{II}{}^{D}$ phase transition in monoelaidin. Mulet et al. investigated the T-scan-induced L_α to $Q_{II}{}^{D}$ phase transition in a synthetic lipid derivative (5′-deoxy-5-fluoro-*N*4-(*cis*-9-octadecycenyloxycarbonyl) cytidine.[27] Using TR-SAXS, they found that the L_α phase converted to the $Q_{II}{}^{D}$ phase without any intermediates in the absence of a copolymer, Poloxamer, when temperature was increased from 25 to 70 °C at a heating rate of 5 °C min^{-1} (33 °C is the phase transition temperature). However, in the presence of Poloxamer, an unidentified intermediate X with a large lattice parameter appeared during the L_α to $Q_{II}{}^{D}$ phase transition. Using cryo-transmission electron microscopy, they also observed the regular arrangement of pores in membranes with Poloxamer when vitrification of samples was performed at 37 °C.[27] Kraneva

dx.doi.org/10.1021/la5021719 | Langmuir 2014, 30, 8131–8140

et al. investigated the P-jump-induced L_α to Q_{II}^G phase transition in MO from 1500 to 1 bar at 20 wt % water.[24] The transition was rapid without any intermediates; that is, the first peak of the Q_{II}^G phase appeared at 1.5 s and the peak of the L_α phase disappeared at 2.5 s, and the spacing of the L_α phase gradually decreased with time by 0.1 nm. Cherezov et al. found that, in T-jump-induced L_α to Q_{II}^D phase transition in *N*-monomethylated dioleoylphosphatidylethanolamine (DOPE-Me) at a final temperature of 61−65 °C, a metastable H_{II} phase formed initially, and disappeared very slowly while the Q_{II} phase developed; after 3 h incubation, both phases coexisted.[23] The kinetics pathway for this system is similar to that of our DOPS/MO system, although the rate constant of the L_α to Q_{II}^D phase transition in our system is much larger than that of the T-jumped transition in DOPE-Me. The third examples are transitions between different Q_{II} phases (i.e., intercubic transitions). Squires et al. investigated the P-jump-induced Q_{II}^G to Q_{II}^D phase transition in a mixture of lauric acid and dilauroylphosphatidylcholine (2:1) (2LA/DLPC) from 600 to 240−360 bar at 50 wt % water.[25] As a long-lived intermediate of the transition, the H_{II} phase appeared. The authors interpreted that the intermediate H_{II} phase is a temporary "water donor" because the water contents of Q_{II}^D phase is larger than that of Q_{II}^G phase, although they did not explain the mechanism of the appearance and disappearance of the H_{II} phase. The first-order rate constants for both the appearance of the Q_{II}^D phase and the disappearance of the Q_{II}^G phase were obtained, which were almost the same. The rate constant decreased with an increase in final pressure (i.e., a decrease in the amount of pressure jump): k = 0.24 and 0.005 s^{-1} for the P-jump from 600 to 240 bar and 600 to 360 bar, respectively. The fourth examples are sponge (L3) to Q_{II} phase transitions. Yaghmur et al. investigated the Ca^{2+}-induced transition from L3 to a mixture of Q_{II}^D and Q_{II}^P phase in a mixture of DOPG and MO.[37] They found that the transition was rapid without any intermediates: for example, 34 mM Ca^{2+}-induced L3 to Q_{II}^D and Q_{II}^P phase transition in 15%-DOPG/85%-MO completed in less than 0.3 s. Although this is the compound-induced phase transition, it is not necessary for Ca^{2+} to diffuse through a lipid membrane to enter a closed vesicle such as the MLV, because in the sponge phase membranes are not closed and do not form a multilayer structure such as the MLV. Thereby, Ca^{2+} can rapidly interact with the lipid membranes to induce the phase transition.

For the T-scan-induced L_α to H_{II} phase transition, a Q_{II} phase appears as an intermediate structure when temperature is increased.[35,38−43] The theory based on only the curvature elastic energy predicts that the $L_\alpha \rightarrow Q_{II} \rightarrow H_{II}$ sequence of phases appears with an increase in temperature.[40,44] Moreover, it is well-known that, for several lipid systems, as water content decreases, the phase sequence is $L_\alpha \rightarrow Q_{II} \rightarrow H_{II} \rightarrow$ inverted micelles (L2).[1,35,45] As we described in our previous paper,[21] from an equilibrium point of view, the most stable phase of the DOPS/MO membrane changes with a decrease in pH according to $L_\alpha \rightarrow Q_{II}^D \rightarrow H_{II}$, because at equilibrium the free energy of the phase determines this sequence. Hence, the phase sequence of the low pH-induced phase transition in the DOPS/MO membrane is the same as that of phase transitions due to the temperature increase or the water content decrease. We can explain the mechanism of low pH-induced phase transition in the DOPS/MO membrane as follows.[21] As pH decreases, the electrostatic interactions due to surface charges of a membrane decrease because of the protonation of the carboxylic group of DOPS. This increases the absolute value of the spontaneous curvature of the monolayer, $|H_0|$, inducing an increase in the Gaussian curvature of the bilayer, $\bar{\kappa}_{bil}$.[12] At the critical value of the electrostatic interactions, $\bar{\kappa}_{bil} = 0$, and the L_α to Q_{II}^D phase transition occurs. Below the critical value of the electrostatic interactions, $\bar{\kappa}_{bil} > 0$ and the Q_{II}^D phase is more stable. Generally, the kinetic pathway of the phase transitions and the structural changes is not the same as the kinetic pathway which follows phases at minimum free energy in the equilibrium state at each conditions, since the kinetics pathway of phase transitions and structural changes is governed by the rate constant, which is determined by the activation energy (or the energy barrier) of the transitions or the structural changes.[46] This general rule is supported by several examples of the kinetic pathway of the phase transitions described above. For the low pH-induced L_α to Q_{II}^D phase transition described in this report, at the pH region (pH 2.6 to 2.8) where the free energy of the Q_{II}^D phase is minimum among the three phases (i.e., L_α, H_{II}, and Q_{II}^D), the Q_{II}^D phase is formed at equilibrium. Between the L_α and the Q_{II}^D phases, there may be several pathways. If the activation energy of the rate-determining step in one kinetic pathway (i.e., the L_α to Q_{II}^D phase transition) is much larger than that in the other kinetic pathway (i.e., the L_α to H_{II} phase transition) (Figure 7), the L_α phase first transforms into the H_{II} phase and then converts to the Q_{II}^D phase. In contrast, if the activation energy of the rate-determining step in the L_α to H_{II} phase transition is much larger than that in the L_α to Q_{II}^D phase transition, the L_α phase transforms directly into the Q_{II}^D phase. It is note that the rate constant also depends on the attempt frequency (e.g., the frequency factor or the pre-exponential factor in the Arrhenius equation of the rate constant), and thereby the difference in the attempt frequency of the rate-determining step of both the pathways may determine the kinetic pathway. Siegel et al. pointed out that the T-change-induced transition from L_α to nonlamellar phases such as Q_{II} and H_{II} phases is determined by kinetic factors (discussed in detail later).[38,39] In the DOPE-Me membrane, the rate of the L_α to Q_{II} and the L_α to H_{II} phase transitions are in kinetic competition.

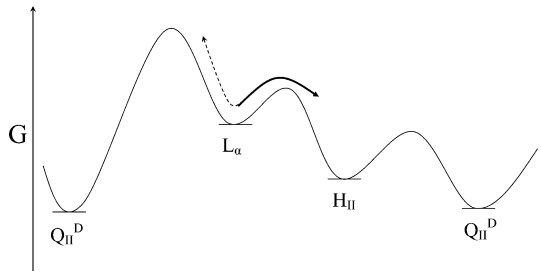

Figure 7. Proposed kinetic pathway for the low pH-induced L_α to Q_{II}^D phase transition. There may be several elementary steps between the two phases, but the rate-determining step governs the total rate of the phase transition. This figure shows only the rate-determining steps in the L_α to Q_{II}^D phase transition and the L_α to H_{II} phase transition. Reprinted from ref 21 with permission from the American Institute of Physics.

Here we propose a hypothesis on the mechanism for this kinetic pathway based on the Siegel model explaining the kinetics pathway of the T-scan-induced L_α to Q_{II} phase transition.[38−40] Thermal fluctuation of bilayers in the L_α phase induces contacts with neighboring bilayers (Figure 8a), and the apposed (cis) monolayers fuse to form stalk structures (Figure 8b), resulting in production of a trans monolayer contact (TMC) (Figure 8c). There are two patterns of structural changes from the TMC. If the trans monolayers at the TMC rupture, an interlamellar

dx.doi.org/10.1021/la5021719 | *Langmuir* 2014, 30, 8131−8140

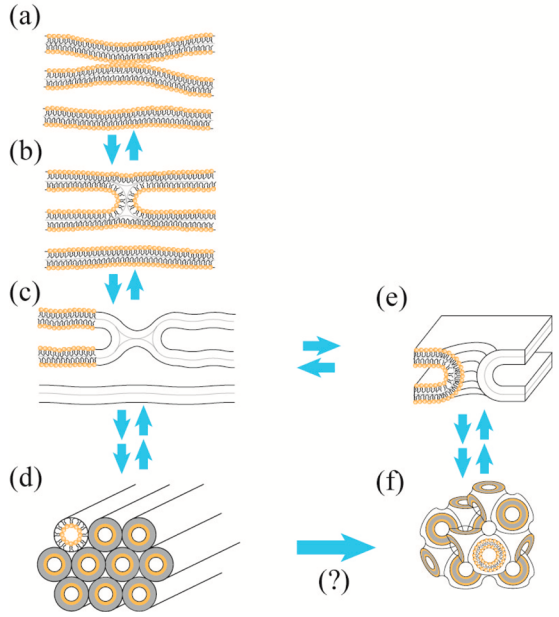

Figure 8. Schematic diagram of the proposed hypothesis for the mechanism controlling the L_α to H_{II} phase transition. (a) Two neighboring bilayers in the L_α phase. (b) A stalk is formed between the bilayers. (c) A trans monolayer contact (TMC) is formed. (d) Formation of the H_{II} phase. (e) If the trans monolayers at the TMC rupture, an interlamellar attachment (ILA) or a fusion pore is formed. (f) Formation of the Q_{II}^D phase.

attachment (ILA) or a fusion pore (Figure 8e) is formed (Type A). If ILAs accumulate in sufficient numbers, they form ILA lattices, which are intermediates in the Q_{II} phase formation (Figure 8f). If no rupture occurs, the TMC or the monolayer cylinder in the membrane accumulates and aggregates (i.e., an H_{II} phase domain), and finally the H_{II} phase appears (Type B) (Figure 8d). In this model, the rupture tension of bilayer σ_r determines the relative rate of the H_{II} phase formation.[39] 20% DOPS/80%MO bilayer may have a large value of σ_r, and thereby the activation energy of the L_α to Q_{II} phase transition is larger than that of the L_α to H_{II} phase transition.[21] However, as the H_{II} phase formation proceeds the strain of the bilayer may increase its tension, inducing its rupture (i.e., ILA formation). This could trigger the H_{II} to Q_{II} phase transition. In our previous paper, we demonstrated that σ_r decreases as the electrostatic interactions due to the surface charges of the membrane increase.[31] With an increase in pH, the surface charge density of the DOPS/MO membrane increases and thereby the electrostatic interactions increase, which induces a decrease in σ_r. This may be one of the factors for decreasing the rate constant of the L_α to the H_{II} phase transition, k_1, with an increase in pH (Table 2, Figure 3c), because the lower rupture tension favors the Type A route. The course-grained molecular dynamics simulation shows one of the models for the transition between the H_{II} and the Q_{II} phases.[41]

Based on the above hypothesis, we considered the dependence of the rate of the conversion of the L_α to the H_{II} phase on the vesicle size or the amounts of the membranes. The process of the formation of the H_{II} phase from the L_α phase can be explained by the classical nucleation theory.[47] According to this theory, the difference of chemical potential of lipid molecules in membranes in between the L_α and the H_{II} phases, $\Delta\mu = \mu(L_\alpha) - \mu(H_{II}) > 0$, induces a small size of the membrane in the H_{II} phase (i.e., an H_{II} phase domain) as a nucleus surrounding the membranes in the L_α phase (i.e., the bulk L_α phase), which decreases the free energy of the total system. However, the interfacial energy between the H_{II} phase domain and the surrounding bulk L_α phase, which includes the deformation energy of the membrane at the interface, increases the free energy of the total system. When the size of the H_{II} phase domain is smaller than a critical size, the effect of the surface of the H_{II} phase domain (i.e., the interfacial energy) is dominant, and thereby the H_{II} phase domain is too unstable to disappear spontaneously. On the other hand, when the size of the H_{II} phase domain is larger than a critical size, the effect of the volume of the H_{II} phase domain (i.e., $\Delta\mu$) is dominant, and thereby the H_{II} phase domain grow spontaneously to complete the L_α to H_{II} phase transition. It has been reported that this nucleation theory can reasonably explain not only crystal growth, where the formation of a crystal nucleus of critical size plays an important role,[48] but also the phase transition in lyotropic liquid crystals.[49,50] Recently, it has been recognized that there are various structures of crystal nucleus. If we assume that the shape of the H_{II} phase domain as a nucleus approximate to a cylinder with a radius r and a length l ($l \gg r$), we calculate the change in Gibbs free energy when an H_{II} phase domain is formed in the surrounding bulk L_α phase,

$$\Delta G = -\pi r^2 ln\ \Delta\mu + 2\pi rl\gamma \tag{5}$$

where n is the density of lipids and γ is the interfacial energy per unit area. At the critical size of the H_{II} phase domain with the critical radius of r^* ($= \gamma/n\Delta\mu$), ΔG has a maximum value of $\Delta G^* = \pi l\gamma^2/n\Delta\mu$, which is called the nucleation barrier or the activation energy. The nucleation rate, J, can be expressed using ΔG^*,

$$J = J_0 \exp(-\Delta G^*/kT) = J_0 \exp(-\pi l\gamma^2/n\Delta\mu kT) \tag{6}$$

where J_0 is the frequency factor, k is Boltzmann constant, and T is absolute temperature. The rate constant of the L_α to the H_{II} phase transition, k_1, increases as J increases. For the 20%-DOPS/80%-MO membrane, $\Delta\mu$ increases with a decrease in pH, because $|H_0|$ increases with a decrease in pH, which induces an increase in k_1. This result is consistent with the experimental results (Table 2, Figure 3c). For the LUVs and the smaller MLVs ~1 μm in diameter, an H_{II} phase domain cannot become larger than the critical size since the number of the bilayers is small in a single vesicle, so they cannot transform into the H_{II} phase. After the LUVs and the smaller MLVs associate and thus increase in size, an H_{II} phase domain can reach the critical size, inducing the transformation of the H_{II} phase. The surface charge density of the DOPS/MO membrane decreases with a decrease in pH,[13] decreasing the electrostatic repulsion between neighboring bilayers. This could increase the rate of formation of the stalk structure and also of the TMC. These events can reasonably explain the experimental result that the rate constant of the conversion of the L_α to the H_{II} phase increased with a decrease in pH. For the LUVs and the smaller MLVs, the rate of the association of the vesicles increased with a decrease in pH (Figure 3d) due to the decrease in the electrostatic repulsion among the vesicles, which also affects the rate constant of the conversion of the L_α to the H_{II} phase.

The T-scan experiments are done under nonequilibrium conditions near the equilibrium, and the T-jump (or P-jump) experiments and our pH-jump experiments in this report are done under nonequilibrium conditions far from the equilibrium. For the phase transitions under such nonequilibrium conditions, there is no theory for their kinetic pathway, and moreover, for several phase transitions neither the structures nor the phases of

dx.doi.org/10.1021/la5021719 | Langmuir 2014, 30, 8131−8140

the intermediates were identified.[25−27] Further experimental and theoretical studies are required in this field.

5. CONCLUSION

The results in this report clearly show the kinetic pathway of the low pH-induced L_α to Q_{II}^D phase transition in 20%-DOPS/80%-MO membranes: first, the L_α phase directly converts into the H_{II} phase in immediate response to the pH-jump (i.e., the initial step), then the H_{II} phase gradually converts into the Q_{II}^D phase. The rate constant of the initial step increased with a decrease in pH and exhibited a large dependence on the vesicle size; for smaller vesicles such as LUVs and smaller MLVs with diameters of ∼1 μm, the rate constant was smaller. These results can be explained by the classical nucleation theory. These data provide the first experimental evidence of the total kinetics of EI-induced L_α/Q_{II} phase transitions. The transient appearance of an intermediate H_{II} phase during the $L_\alpha \rightarrow Q_{II}$ transition is a new kinetic pathway of phase transitions of lipid membranes. It is indispensable to develop quantitative theories and computer simulations on the kinetics of EI-induced L_α/Q_{II} phase transitions.

AUTHOR INFORMATION

Corresponding Author

*Mailing address: Nanomaterials Research Division, Research Institute of Electronics, Shizuoka University, 836 Oya, Suruga-ku, Shizuoka 422-8529, Japan. Tel/Fax: 81-54-238-4741. E-mail: spmyama@ipc.shizuoka.ac.jp.

Notes

The authors declare no competing financial interest.

ACKNOWLEDGMENTS

This work was supported by a Grant-in-Aid for Scientific Research in Priority Areas (Soft Matter Physics) (No. 21015009) from the Ministry of Education, Culture, Sports, and Science to M.Y. The synchrotron radiation experiments were performed using BL40B2 and BL45XU at SPring-8 with the approval of the Japan Synchrotron Radiation Research Institute (JASRI) (Proposal No. 2010B1245, 2011A1188, 2011A1190, 2011B1249, 2011B1880, 2012A1305, 2012A1655, 2012B1191, 2012B1763, 2013A1252, 2013A1228, 2013B1266, 2014A1180). This work was partially carried out using an instrument at the Center for Instrumental Analysis, Shizuoka University, Japan.

REFERENCES

(1) Seddon, J. M.; Templer, R. H. Polymorphism of lipid-water systems. In *Structure and dynamics of membranes*; Lipowsky, R., Sackmann, E., Eds.; Elsevier Science B. V.: Amsterdam, 1995; pp 97−160.

(2) Luzzati, V. Biological significance of lipid polymorphism: the cubic phases. *Curr. Opin. Struct. Biol.* **1997**, *7*, 661−668.

(3) Schwarz, U. S.; Gompper, G. Stability of inverse bicontinuous cubic phases in lipid-water mixtures. *Phys. Rev. Lett.* **2000**, *85*, 1472−1475.

(4) Almsherqi, Z. A.; Kohlwein, S. D.; Deng, Y. Cubic membranes: a legend beyond the Flatland of cell membrane organization. *J. Cell Biol.* **2006**, *173*, 839−844.

(5) Aota-Nakano, Y.; Li, S. J.; Yamazaki, M. Effects of electrostatic interaction on the phase stability and structures of cubic phases of monoolein/oleic acid mixture membranes. *Biochim. Biophys. Acta* **1999**, *1461*, 96−102.

(6) Li, S. J.; Yamashita, Y.; Yamazaki, M. Effect of Electrostatic interactions on phase stability of cubic phases of membranes of monoolein/dioleoylphosphatidic acid mixture. *Biophys. J.* **2001**, *81*, 983−993.

(7) Cherezov, V.; Clogston, J.; Misquitta, Y.; Abdel-Gawad, W.; Caffrey, M. Membrane protein crystallization in meso: lipid type-tailoring of the cubic phase. *Biophys. J.* **2002**, *83*, 3393−3407.

(8) Chupin, V.; Killian, J. A.; de Kruijff, B. Effect of phospholipids and a transmembrane peptides on the stability of the cubic phase of monoolein: implication for protein crystallization from a cubic phase. *Biophys. J.* **2003**, *84*, 2373−2381.

(9) Masum, S. M.; Li, S. J.; Tamba, Y.; Yamashita, Y.; Tanaka, T.; Yamazaki, M. Effect of de novo designed peptides interacting with the lipid-membrane interface on the stability of the cubic phases of the monoolein membrane. *Langmuir* **2003**, *19*, 4745−4753.

(10) Masum, S. M.; Li, S. J.; Awad, T. S.; Yamazaki, M. Effect of positively charged short peptides on stability of cubic phases of monoolein/dioleoylphosphatidic acid mixtures. *Langmuir* **2005**, *21*, 5290−5297.

(11) Awad, T. S.; Okamoto, Y.; Masum, S. M.; Yamazaki, M. Formation of cubic phases from large unilamellar vesicles of dioleoylphosphatidylglycerol/monoolein membranes induced by low concentrations of Ca^{2+}. *Langmuir* **2005**, *21*, 11556−11561.

(12) Yamazaki, M. Transformation between Liposomes and Cubic Phases of Biological Lipid Membranes Induced by Modulation of Electrostatic Interactions. *Adv. Planar Lipid Bilayers Liposomes* **2009**, *9*, 163−209.

(13) Okamoto, Y.; Masum, S. M.; Miyazawa, H.; Yamazaki, M. Low pH-induced transformation of bilayer membrane into bicontinuous cubic phase in dioleoyl-phosphatidylserine/monoolein membranes. *Langmuir* **2008**, *24*, 3400−3406.

(14) Pisani, M.; Fine, V.; Bruni, P.; Cola, E. D.; Francescangeli, O. Metal cation induced cubic phase in poly(ethylene glycol)-functionalized dioleoylphosphatidylethanolamine aqueous dispersions. *J. Phys. Chem. B* **2008**, *112*, 5276−5278.

(15) Efrat, R.; Aserin, A.; Garti, N. On structural transitions in a discontinuous micellar cubic phase loaded with sodium diclofenac. *J. Colloid Interface Sci.* **2008**, *321*, 166−176.

(16) Silva, J. P. N.; Oliveira, R.; Coutinho, P. J. G. Characterization of mixed DODAB/monoolein aggregates using Nile Red as a solvatochromic and anisotropy fluorescent probe. *J. Photochem. Photobiol., A* **2009**, *203*, 32−39.

(17) Efrat, R.; Abramov, Z.; Aserin, A.; Garti, N. Nonionic-anionic mixed surfactants cubic mesophases. Part I: Structural chaotropic and kosmotropic effect. *J. Phys. Chem. B* **2010**, *114*, 10709−10716.

(18) Muir, B. W.; Zhen, G.; Gunatillake, P.; Hartley, P. G. Salt induced lamellar to bicontinuous cubic phase transitions in cationic nanoparticles. *J. Phys. Chem. B* **2012**, *116*, 3551−3556.

(19) Oliveria, I. M. S. C.; Silv, J. P. N.; Feitos, E.; Marques, E. F.; Castanheira, E. M. S.; Oliveira, M. E. C. D. R. Aggregation behaviour of aqueous dioctadecyldimethylammonium bromide/monoolein mixtures: A multitechnique investigation on the influence of composition and temperature. *J. Colloid Interface Sci.* **2012**, *374*, 206−217.

(20) Liu, Q.; Dong, Y.-D.; Hanley, T. L.; Boyd, B. J. Sensitivity of nanostructure in charged cubosomes to phase changes triggered by ionic species in solution. *Langmuir* **2013**, *29*, 14265−14273.

(21) Alam, M. M.; Oka, T.; Ohta, N.; Yamazaki, M. Kinetics of Low pH-Induced Lamellar to Bicontinuous Cubic Phase Transition in Dioleoylphosphatidylserine/Monoolein. *J. Chem. Phys.* **2011**, *134* (145102), 10 pages.

(22) Squires, A. M.; Templer, R. H.; Seddon, J. M.; Woenckhaus, J.; Winter, R.; Finet, S.; Theyenchei, N. Kinetics and mechanism of the lamellar to gyroid inverse bicontinuous cubic phase transition. *Langmuir* **2002**, *18*, 7384−7392.

(23) Cherezov, V.; Siegel, D. P.; Shaw, W.; Burgess, S. W.; Caffrey, M. The kinetics of non-lamellar phase formation in DOPE-Me: relevance to biomembrane fusion. *J. Membr. Biol.* **2003**, *195*, 165−182.

(24) Kraineva, J.; Narayanan, R. A.; Kondrashkina, E.; Thyagarajan, P.; Winter, R. Kinetics of lamellar-to-cubic and intercubic phase transitions of pure and cytochrome c containing monoolein dispersions monitored by time-resolved small-angle X-ray diffraction. *Langmuir* **2005**, *21*, 3559−3571.

(25) Squires, A. M.; Templer, R. H.; Seddon, J. M.; Woenckhaus, J.; Winter, R.; Narayanan, T.; Finet, S. Kinetics and mechanism of interconversion of inverse bicontinuous cubic mesophase. *Phys. Rev. E* **2005**, *72* (011502), 16 pages.
(26) Conn, C. E.; Ces, O.; Mulet, X.; Finet, S.; Winter, R.; Seddon, J. M.; Templer, R. H. Dynamics of structural transformations between lamellar and inverse bicontinuous cubic lyotropic phases. *Phys. Rev. Lett.* **2006**, *96*, 108102.
(27) Mulet, X.; Gong, X.; Waddington, L. J.; Drummond, C. J. Observing self-assembled lipid nanoparticles building order and complexity through low-energy transformation processes. *ACS Nano* **2009**, *3*, 2789−2797.
(28) Angelova, A.; Angelov, B.; Garamus, V. M.; Couvreur, P.; Lesieur, S. Small-angle X-ray scattering investigations of biomolecular confinement, loading, and release from liquid-crystalline nanochannel assemblies. *J. Phys. Chem. Lett.* **2012**, *3*, 445−457.
(29) Paatero, P.; Tapper, U. Positive matrix factorization: A non-negative factor model with optimal utilization of error estimates of data values. *Environmetrics* **1994**, *5*, 111−126.
(30) Wang, J.-H.; Hopke, P.K.; Hancewicz, T. M.; Zhang, S. L. Application of modified alternating least squares regression to spectroscopic image analysis. *Anal. Chimi. Acta* **2003**, *476*, 93−109.
(31) Levadny, V.; Tsuboi, T.; Belaya, M.; Yamazaki, M. Rate constant of tension-induced pore formation in lipid membranes. *Langmuir* **2013**, *29*, 3848−3852.
(32) Pabst, P. Global properties of biomimetic membranes: perspectives on molecular features. *Biophys. Rev. Lett.* **2006**, *1*, 57−84.
(33) Pozo-Navas, B.; Raghunathan, V. A.; Katsaras, J.; Rappolt, M.; Lohner, K.; Pabst, G. Discontinuous unbinding of lipid multibilayers. *Phys. Rev. Lett.* **2003**, *91*, 02801.
(34) Tate, M. W.; Shyamsunder, E.; Gruner, S. M.; D'Amico, K. L. Kinetics of the lamellar-inverse hexagonal phase transition determined by time-resolved X-ray diffraction. *Biochemistry* **1992**, *31*, 1081−1092.
(35) Seddon, J. M. Structure of the inverted hexagonal (H_{II}) phase, and non-lamellar phase transitions of lipids. *Biochim. Biophys. Acta* **1990**, *1031*, 1−69.
(36) Paul, S.; Volkov, A. G.; Van Hoek, A. N.; Haines, T. H.; Deamer, D. W. Permeation of protons, potassium ions, and small polar molecules through phospholipid bilayers as a function of membrane thickness. *Biophys. J.* **1996**, *70*, 339−348.
(37) Yaghmur, A.; Sartori, B.; Rappolt, M. The role of calcium in membrane condensation and spontaneous curvature variations in model lipidic systems. *Phys. Chem. Chem. Phys.* **2011**, *13*, 3115−3225.
(38) Siegel, D. P.; Epand, R. M. The mechanism of lamellar-to-inverted hexagonal phase transitions in phosphatidylethanolamine: implications for membrane fusion mechanisms. *Biophys. J.* **1997**, *73*, 3089−3111.
(39) Siegel, D. P. The modified stalk mechanism of lamellar/inverted phase transitions and its implications for membrane fusion. *Biophys. J.* **1999**, *76*, 291−313.
(40) Siegel, D. P.; Kozlov, M. M. The Gaussian curvature elastic modulus of N-monomethylated dioleoylphosphatidylethanolamine; relevance to membrane fusion and lipid phase behaviour. *Biophys. J.* **2004**, *87*, 366−374.
(41) Marrink, S.-J.; Tieleman, D. P. Molecular dynamics simulation of spontaneous membrane fusion during a cubic-hexagonal phase transition. *Biophys. J.* **2002**, *83*, 2386−2392.
(42) Koynova, R.; Caffrey, M. Phase and phase-transitions of the hydrated phosphatidylethanolamines. *Chem. Phys. Lipids* **1994**, *69*, 1−34.
(43) Shyamsunder, E.; Gruner, S. M.; Tate, M. W.; Turner, D. C.; So, P. T. C.; Tilcock, C. P. S. Observation of inverted cubic phases in hydrated dioleoylphosphatidylethanolamine membranes. *Biochemistry* **1988**, *27*, 2332−2336.
(44) Siegel, D. P.; Tenchov, B. G. Influence of the lamellar phase unbinding energy on the relative stability of lamellar and inverted cubic phases. *Biophys. J.* **2008**, *94*, 3987−3995.
(45) Yaghmur, A.; Rappolt, M.; Østergaard, J.; Larsen, C.; Larsen, S. W. Characterization of bupivacaine-loaded formulations based on liquid crystalline phases and microemulsions: the effect of lipid composition. *Langmuir* **2012**, *28*, 2881−2889.
(46) For example, Hajduk, D. A.; Ho, R.-M.; Hillmyer, M. A.; Bates, F. S.; Almdal, K. Transition mechanisms for complex ordered phases in block copolymer melts. *J. Phys. Chem. B* **1998**, *102*, 1356−1363. Iwashita, Y.; Tanaka, H. Spontaneous onion-structure formation from planar lamellar nuclei. *Phys. Rev. Lett.* **2007**, *98*, 145703.
(47) For example, Debenedetti, P. G. *Metastable Liquids*; Princeton University Press: Princeton, NJ, 1996.
(48) For example, Saito, Y. *Statistical Physics of Crystal Growth*; World Scientific: Singapore, 1996.
(49) Dogic, Z. Surface freezing and a two-step pathway of the isotropic-smectic phase transition in colloidal rods. *Phys. Rev. Lett.* **2003**, *91*, 165701.
(50) Zanchetta, G.; Nakata, M.; Buscaglia, M.; Bellini, T.; Clark, N. A. Phase separation and liquid crystallization of complementary sequences in mixtures of nano DNA oligomers. *Proc. Natl. Acad. Sci. U.S.A.* **2008**, *105*, 1111−1117.